R. & M. No. 3674

R. & M. No. 3674

MINISTRY OF DEFENCE

AERONAUTICAL RESEARCH COUNCIL
REPORTS AND MEMORANDA

An Approximate Analysis of the Non-Linear Lateral Motion of a Slender Aircraft (HP 115) at Low Speeds

By A. JEAN ROSS and L. J. BEECHAM

Aero Dept., R.A.E. Farnborough

LONDON: HER MAJESTY'S STATIONERY OFFICE

1971

PRICE £1·25 NET

An Approximate Analysis of the Non-Linear Lateral Motion of a Slender Aircraft (HP 115) at Low Speeds

By A. JEAN ROSS and L. J. BEECHAM

Aero Dept., R.A.E. Farnborough

Reports and Memoranda No. 3674*
May, 1970

Summary.

An approximate analytical method is developed for the solution of a fourth order, non-linear equation of motion from which the frequency and amplitude of a sustained oscillation may be derived. The criterion for the existence of the limit cycle is a modified form of Routh's discriminant, its sign, and the sign of its derivative with respect to the square of the instantaneous amplitude. Comparisons at spot points show excellent agreement with 'exact' digital computations.

The method has been applied to the lateral motion limit cycle encountered at low speeds on the HP 115 aircraft, and comparisons with the results of wind tunnel dynamic simulations show that the onset and nature of the sustained oscillation is predicted very satisfactorily.

LIST OF CONTENTS

*Replaces R.A.E. Tech. Report No. 70085—A.R.C. 32 345.

---

1. *Introduction.*

In Ref. 1 an account was given of a simulation exercise on the HP 115 aircraft at low speed and high incidence conditions which in full scale flight produced a sustained oscillation in the Dutch roll mode. This exercise put to the test a novel simulator facility in which part of the aerodynamic loads—the forces and moments due to the angle between the body and flight-path axes—was supplied in an analogue form directly from a wind tunnel balance, thereby eliminating the mathematical modelling of these terms. The simulation reproduced the flight behaviour, showing a normal convergent Dutch roll at moderate angles of attack, and at higher angles the sustained oscillations, of an amplitude increasing with angle of attack.

There was some weak coupling between the longitudinal and lateral modes; for example, there was some excitation in pitch around the trim angle of attack, which itself produced a cyclic change of the Dutch roll amplitude. But these effects were small enough to suggest that the motion should be amenable to analytic treatment by consideration of a fourth order system in which due allowance is made for non-linearities, viz

$$\frac{d^4x}{dt^4}+\frac{d^3A(x)}{dt^3}+\frac{d^2B(x)}{dt^2}+\frac{dC(x)}{dt}+D(x)=0\,. \tag{1}$$

In Ref. 2 an approximate method of treating second order systems of the type $\ddot{x}+F(x,\dot{x})=0$ was given. The approximation produces a solution, not of $x(t)$, but of the frequency and amplitude damping

envelope as a function of the amplitude. The difficulties escalate as the order of the equation is increased. But to offset this, many of the awkward terms disappear in the special case of a steady sustained oscillation, and so the method seemed to offer a powerful way of formulating the conditions under which such oscillations could occur.

The Report develops the method and applies it to the particular case of the HP 115 slender aircraft.

2. *Method.*

2.1. *General.*

We are concerned with non-linear dynamic systems with an autonomous response similar in type to that of a linear system, viz an identifiable (but not necessarily constant) frequency and an amplitude varying with time. It is logical therefore to look for an approximate solution consisting of a summation of terms with separable real and imaginary parts, reflecting the time dependence of the amplitude and frequency respectively, viz

$$x = \Sigma\, \theta(t)\, e^{i\phi(t)}\,. \tag{2}$$

The parallel with the special case of the linear system is then clear inasmuch as in this case $\theta(t) = \theta_0\, e^{at}$ and $\phi(t) = bt$ where a and b are constants. If some terms in the summation have no imaginary part we have the equivalent of divergent and convergent modes.

For an 'm'th order system in which differentials up to d^m/dt^m appear, we choose that there are 'm' terms in the summation for x, again in parallel with the linear solution. Up to this point no generality has been lost, because, by virtue of the fact that superposition of solutions does not apply for non-linear equations, the terms in the summation of equation (2) may be mutually dependent.

We now introduce the approximation that we may disregard any transfer of energy between the various modes so that the solution may be regarded as a summation of mutually independent terms, the number being appropriate to the order of the differential equation, which are unknown functions of time.

Then, if we write

$$\lambda = \frac{\dot{\theta}}{\theta},$$

$$\omega = \dot{\phi}\,,$$

and

$$Z = \lambda + i\omega$$

we have

$$\left.\begin{aligned} x &= \sum_1^m \theta_n\, e_i^{\phi n} \\ \dot{x} &= \sum_1^m \theta_n\, e^{i\phi n}\, Z_n \\ \ddot{x} &= \sum_1^m \theta_n\, e^{i\phi n}\, (Z_n^2 + R_{2n}) \\ \frac{d^r x}{dt^r} &= \sum_1^m \theta_n\, e^{i\phi n}\, (Z_n^r + R_{rn}) \end{aligned}\right\} \tag{3}$$

where $R_2 = \lambda\,\theta\,Z'$

$$R_3 = \lambda\,\theta\,[2Z' + \lambda\,\theta\,Z'' + (\lambda'\,\theta + \lambda)\,Z'] \text{ etc.}$$

the primes denoting $\frac{d}{d\theta}$.

R_2 corresponds to the form of solution adopted in Ref. 2 for a second order system.

Since we have disregarded any periodic energy interchange between modes, a steady state exists only when $\lambda_n = 0$, i.e. $R_n = 0$, in which case equation (3) takes a particularly simple form. The divergent/convergent modes will have reached a constant value and the oscillatory modes a sustained amplitude.

2.2. *Specific Application.*

We now consider the application to a fourth order system representing the lateral stability equation for a particular aircraft in which we prescribe that there is the usual one oscillatory mode (the Dutch roll) and two first order modes (i.e. the spiral and roll subsidence modes), so that

$$x = [\theta_1 + \theta_2]\,(t) \cos \phi(t) + \theta_3(t) + \theta_4(t)\,.$$

In Section 3.3.2 the full expressions corresponding to equation (3) have been used to investigate the growth of the dutch roll amplitude, but the main body of the present report is concerned with conditions only in the terminal state. In this condition

$$\theta_3 + \theta_4 = \text{constant} = \Theta_0, \text{ say}$$

$$\theta_1 + \theta_2 = \text{constant} = \Theta\ , \text{say}$$

whence

$$\left.\begin{aligned} x &= \Theta \cos \phi + \Theta_0 \\ \dot{x} &= -\omega\,\Theta \sin \phi \\ \ddot{x} &= -\omega^2\,\Theta \cos \phi \\ \dddot{x} &= \omega^3\,\Theta \sin \phi \\ \ddddot{x} &= \omega^4\,\Theta \cos \phi\,. \end{aligned}\right\} \tag{4}$$

Let the general term in equation (1) be $P(x)$ and a polynomial in x, so that $P(x) = \Sigma\, p_n\, x^n$. Then because of the lateral symmetry of the aircraft, the coefficients of even powers of x are zero, and we are therefore concerned with repeated time derivatives of polynomials of the form $\Sigma\, p_{2n+1}\, x^{2n+1}$, i.e.

$$\left.\begin{aligned} P(x) &= \sum_0^N p_{2n+1}\, x^{2n+1} \\ \frac{dP}{dt} &= \sum p_{2n+1}\,(2n+1)\,x^{2n}\,[\dot{x}] \\ \frac{d^2P}{dt^2} &= \sum p_{2n+1}\,(2n+1)\,x^{2n-1}\,[2n(\dot{x})^2 + x\,\ddot{x}] \\ \frac{d^3P}{dt^3} &= \sum p_{2n+1}\,(2n+1)\,x^{2n-2}\,[2n(2n-1)\,(\dot{x})^3 + 6n\,x\,\dot{x}\,\ddot{x} + x^2\,\dddot{x}]\,. \end{aligned}\right\} \tag{5}$$

Substituting for equation (4) in (5) we may rewrite equation (1) as:

$$\omega^4 \Theta \cos\phi +$$

$$+\omega^3 \Theta \sin\phi \Sigma a_{2n+1} (2n+1)(\Theta\cos\phi+\Theta_0)^{2n-2}\Big[(\Theta\cos\phi+\Theta_0)^2+6n\,\Theta\cos\phi(\Theta\cos\phi+\Theta_0)-$$

$$-\Theta^2 2n(2n-1)\sin 2\phi\Big]-$$

$$-\omega^2 \Theta \Sigma b_{2n+1}(2n+1)(\Theta\cos\phi+\Theta_0)^{2n-1}[2n\Theta\sin^2\phi+(\Theta\cos\phi+\Theta_0)\cos\phi]+$$

$$-w\,\Theta\sin\phi\,\Sigma c_{2n+1}(2n+1)(\theta\cos\phi-\Theta_0)^{2n}+$$

$$+\Sigma d_{2n+1}(\Theta\cos\phi+\Theta_0)^{2n+1}$$

$$=0. \tag{6}$$

We next make use of the fact that if $f \equiv f(\sin\phi, \cos\phi) = 0$, then

$$\int_0^{2\pi} f.\sin^p\phi\,d\phi = 0 = \int_0^{2\pi} f.\cos^p\phi\,d\phi.$$

In Ref. 2, the two equations corresponding to $p = 1$ were used which were sufficient to solve fully the second order system for the knknown λ and ω. Here by analogy we use $p = 1$ and 2 to derive the necessary and sufficient equations. Taking firstly $p = 2$, we have,

$$\Theta_0\left\{-\omega^2 \sum_{n=1} b_{2n+1}(2n+1)K_3(n)+\sum_{n=0} d_{2n+1}K_1(2n+1)\right\}=0,$$

and

$$\Theta_0\left\{\omega^2 \sum_{n=1} b_{2n+1}(2n+1)K_3(n)+\sum_{n=0} d_{2n+1}K_2(2n+1)\right\}=0,$$

where

$$K_3(n) = -(2n)!\sum_{l=1}^{n}\frac{\Theta_0^{2n-2l}\Theta^{2l}}{(2n+1-2l)!\,(l-1)!\,(l+1)!\,2^{2l-2}}$$

$$K_1(2n+1) = (2n+1)!\sum_{l=0}^{n}\frac{\Theta_0^{2n-2l}\Theta^{2l}}{(2n+1-2l)!\,(l+1)!\,l!\,2^{2l}}$$

$$K_2(2n+1) = (2n+1)!\sum_{l=0}^{n}\frac{\Theta_0^{2n-2l}\Theta^{2l}(2l+1)!}{(2n+1-2l)!\,(l+1)!\,l!\,2^{2l}}$$

so that either

$$\Theta_o = 0 \tag{7}$$

or

$$\sum_{n=0} d_{2n+1}(2n+1)!\sum_{l=0}^{n}\frac{\Theta_0^{2n-2l}\Theta^{2l}}{(2n+1-2l)!\,l!\,l!\,2^{2l-1}}=0. \tag{8}$$

It is found that the frequency resulting from equation (8) for the particular aircraft under consideration is imaginary so that only equation (7) is a valid solution.

This effects a considerable simplification of equation (6) which, after the subsequent integrations using $p = 1$, leads to the following:-

$$\omega^2 \left\{ a_1 + \sum_{n=1} a_{2n+1} X(n) \Theta^{2n} \right\} = c_1 + \sum_{n=1} c_{2n+1} X(n) \Theta^{2n} \tag{9}$$

and

$$\omega^4 - \omega^2 \left\{ b_1 + \sum_{n=1} b_{2n+1} X(n) \Theta^{2n} \right\} + \left\{ d_1 + \sum_{n=1} d_{2n+1} X(n) \Theta^{2n} \right\} = 0 \tag{10}$$

where

$$X(n) = \frac{(2n+1)!}{2^{2n} n! (n+1)!}.$$

Equations (9) and (10) suffice to determine the frequency and amplitude of the sustained oscillation, and the conditions under which the latter occurs. Eliminating ω^2 from equations (9) and (10) enables the expression for the amplitude to be written in the form:

$$-[c_1 + \sum_1 c_{2n+1} X(n) \Theta^{2n}]^2 +$$

$$+ [c_1 + \sum_1 c_{2n+1} X(n) \Theta^{2n}] [b_1 + \sum_1 b_{2n+1} X(n) \Theta^{2n}] [a_1 + \sum_1 a_{2n+1} X(n) \Theta^{2n}] -$$

$$- [a_1 + \sum_1 a_{2n+1} X(n) \Theta^{2n}]^2 [d_1 + \sum_1 d_{2n+1} X(n) \Theta^{2n}] = 0, \tag{11}$$

that is, Routh's discriminant for an equivalent linear system formed by replacing a_1, b_1, etc., applicable to the linear case by $[a_1 + \sum_1 a_{2n+1} X(n) \Theta^{2n}]$, $[b_1 + \sum_1 b_{2n+1} X(n) \Theta^{2n}]$, etc. The amplitude of the sustained (non-linear) oscillation is then given by the condition that the equivalent linear system is neutrally stable.

In Ref. 2 it was shown that for a non-linear second order system of the type considered there exists an equivalent linear system, (the equivalence being a function of amplitude), which has the same frequency and damping. The equivalent stiffness, $\bar{S}$, is the dynamic mean defined by $\bar{S} = \frac{1}{\pi} \int_0^{2\pi} S(x) \sin^2 \phi \, d\phi$. The physical significance of the replacement terms, $[a_1 + \sum_1 a_{2n+1} X(n) \Theta^{2n}]$ etc., in Routh's discriminant is that they are the dynamic means of the slopes of $A(x)$, $B(x)$, etc. similarly obtained.

Thus, at least in systems such as that presently considered in which there is only one sustained oscillation, the existence, frequency and amplitude of this oscillation may be determined directly merely by formulating the modified Routh's discriminant, R, using the dynamic mean of each of $A(x)$, $B(x)$, etc. Then, since $R = R_{\theta=0} + \Theta^2 \left(\frac{\partial R}{\partial(\Theta^2)} \right)_{\theta=0} + \ldots = 0$

$$\Theta^2 \approx \left[\frac{-R}{\frac{\partial R}{\partial(\Theta^2)}} \right]. \tag{12}$$

The existence is determined by the range of Θ for which R and $\dfrac{\partial R}{\partial(\Theta^2)}$ are of opposite sign.

3. *Application to Simulation of HP 115 Aircraft.*

The model of the HP 115 aircraft tested in the wind tunnel/flight dynamics simulator, to investigate its lateral behaviour, was also free to respond longitudinally, but the resulting change in angle of attack was regarded as sufficiently small for the longitudinal response to be neglected in the basic theoretical treatment. However, due account has been taken of the effect of this cross-coupling back onto the lateral behaviour where necessary, e.g. Sections 3.3.1 and 3.3.2.

The lateral equations of motion of an aircraft, flying at a given speed (or angle of attack), are usually expressed in terms of perturbations in sideslip velocity, roll rate and yaw rate, with aerodynamic forces and moments approximated by their first derivatives with respect to the perturbations. In the simulation of the motion of the HP 115 aircraft in the wind tunnel, the forces and moments due to roll rate and yaw rate were represented in this manner, but the sideforce, rolling moment and yawing moment due to sideslip velocity were obtained directly from wind-tunnel measurements. Examination of the static wind-tunnel tests shows that the sideforce and rolling moment are almost linearly dependent on sideslip velocity, but that the yawing moment is distinctly non-linear.

Representation of the yawing moment coefficient, C_n, in the form $C_n = n_1\,\bar{v} + n_3\,\bar{v}^3$ gave good agreement with the experimental values, where n_1 and n_3 are dependent on the angle of attack, and were calculated to give the best mean curve through the data. A comparison of the sideforce and moments due to sideslip and their approximate values at a relatively high angle of attack, $\bar{w} = 0{\cdot}25$, is shown in Fig. 1, and the variation of y_v, l_v, n_1 and n_3 with angle of attack is shown in Fig. 2.

3.1. *Equations of Motion.*

The lateral equations of motion, when the yawing moment due to sideslip is non-linear, may be written as:—

$$\left.\begin{aligned}
\frac{d\bar{v}}{dt} - \bar{w}\,p + r - \frac{g}{V}\varphi &= \frac{\rho S V^2}{m}\left(y_v\,\bar{v} + y_p\frac{ps}{V} + y_r\frac{rs}{V}\right)\\
\frac{dp}{dt} + e_x\frac{dr}{dt} &= \frac{\rho S V^2 s}{I_x}\left(l_v\,\bar{v} + l_p\frac{ps}{V} + l_r\frac{rs}{V}\right)\\
\frac{dr}{dt} + e_z\frac{dp}{dt} &= \frac{\rho S V^2 s}{I_z}\left(n_1\,\bar{v} + n_3\,\bar{v}^3 + n_p\frac{ps}{V} + n_r\frac{rs}{V}\right)\\
p - \frac{d\varphi}{dt} &= 0
\end{aligned}\right\} \qquad (13)$$

By elimination of p, r and φ, the differential equation for $\bar{v}$ is obtained in a form similar to that of equation (1), viz:

$$\frac{d^4\bar{v}}{dt^4} + \frac{d^3A(\bar{v})}{dt^3} + \frac{d^2B(\bar{v})}{dt^2} + \frac{dC(\bar{v})}{dt} + D(\bar{v}) = 0$$

where

$$\begin{aligned}
A(\bar{v}) &= a_1\,\bar{v}\\
&= -\left(\frac{\rho S V}{m}\right)\left[y_v + \frac{1}{(1-e_x e_z)}\left\{\frac{l_p}{i_x} + \frac{n_r}{i_z} - \frac{e_x n_p}{i_z} - \frac{e_z l_r}{i_x}\right\}\right]\bar{v}
\end{aligned} \qquad (14)$$

$$B(\bar{v}) = b_1\,\bar{v}+b_3\,\bar{v}^3$$

$$=\left(\frac{\rho SV}{m}\right)^2\left[\frac{1}{i_x\,i_z}(l_p\,n_r-n_p\,l_r)+y_v\left\{\frac{l_p}{i_x}+\frac{n_r}{i_z}-\frac{e_x\,n_p}{i_z}-\frac{e_z\,l_r}{i_x}\right\}-\right.$$

$$\left.-\frac{l_v}{i_x}\left\{\frac{m}{\rho Ss}(\bar{w}+e_z)+y_p-e_z\,y_r\right\}+\frac{n_1}{i_z}\left\{\frac{m}{\rho Ss}(1+e_z\,\bar{w})-y_r+e_x\,y_p\right\}\right]\frac{\bar{v}}{(1-e_x\,e_z)}+$$

$$+\left(\frac{\rho SV}{m}\right)^2\left[\frac{m}{\rho Ss}(1+e_x\,\bar{w})-y_r+e_x\,y_p\right]\frac{n_3\,\bar{v}^3}{i_z\,(1-e_x\,e_z)} \tag{15}$$

$$C(\bar{v}) = c_1\,\bar{v}+c_2\,\bar{v}^3$$

$$= -\left(\frac{\rho SV}{m}\right)^3\left[y_v\,(l_p\,n_r-n_p\,l_r)-l_v\left\{\frac{m}{\rho Ss}\left(n_p+\bar{w}\,n_r+i_z\frac{C_z}{2}\right)+y_p\,n_r-y_r\,n_p\right\}+\right.$$

$$\left.+n_1\left\{\frac{m}{\rho Ss}\left(l_p+\bar{w}\,l_r-i_{xz}\frac{C_z}{2}\right)+y_p\,l_r-y_r\,l_p\right\}\right]\frac{\bar{v}}{i_x\,i_z\,(1-e_x\,e_z)}-$$

$$-\left(\frac{\rho SV}{m}\right)^3\left[\frac{m}{\rho Ss}\left(l_p+\bar{w}\,l_r-i_{xz}\frac{C_z}{2}\right)+y_p\,l_r-y_r\,l_p\right]\frac{n_3\,\bar{v}^3}{i_x\,i_z\,(1-e_x\,e_z)} \tag{16}$$

$$D(\bar{v}) = d_1\,\bar{v}+d_3\,\bar{v}^3$$

$$= -\left(\frac{\rho SV}{m}\right)^4\frac{m}{\rho Ss}\frac{C_z}{2}(l_v\,n_r-n_1\,l_r)\frac{\bar{v}}{i_x\,i_z\,(1-e_x\,e_z)}+$$

$$+\left(\frac{\rho SV}{m}\right)^4\frac{m}{\rho Ss}\frac{C_z}{2}\frac{l_r\,n_3\,\bar{v}^3}{i_x\,i_z\,(1-e_x\,e_z)}. \tag{17}$$

As is customary, $i_x = \dfrac{I_x}{ms^2}$ etc., $e_x = -\dfrac{I_{xz}}{I_x}$, $e_z = -\dfrac{I_{xz}}{I_z}$ and $C_z \approx -\dfrac{mg}{\frac{1}{2}\rho V^2 S}$ for the range of $\bar{w}$ currently considered. The coefficients a_1, a_3 etc. are shown in Fig. 3 for the range of $\bar{w}$, and the values of the inertias etc. are given in the table.

The equivalent coefficients introduced in equation (11) are thus given by:

$$\left.\begin{aligned} a^* &= a_1 \\ b^* &= b_1+\tfrac{3}{4}b_3\,\Theta^2 \\ c^* &= c_1+\tfrac{3}{4}c_3\,\Theta^2 \\ d^* &= d_1+\tfrac{3}{4}d_3\,\Theta^2 \end{aligned}\right\} \tag{18}$$

where the coefficients b_3, c_3 and d_3 are each proportional to the non-linear contribution n_3. The equivalent Routh's discriminant, $R^* = a^*\,b^*\,c^*-a^{*2}\,d^*-c^{*2} = 0$, then leads to a quadratic for Θ^2, which has the approximate solution,

$$\Theta^2 \approx \tfrac{3}{4}\frac{[c_1^2-a_1\,b_1\,c_1+a_1^2\,d_1]}{[a_1\,b_1\,c_3+a_1\,b_3\,c_1-a_1^2\,d_3-2c_1\,c_3]} \tag{19}$$

and from equation (9),

$$\omega^2 = c^*/a_1 . \tag{20}$$

Alternatively, Θ^2 may be eliminated to give a quadratic for ω^2,

$$\omega^4\left(1-\frac{b_3 a_1}{c_3}\right)-\omega^2\left(b_1-\frac{b_3 c_1}{c_3}-\frac{d_3 a_1}{c_3}\right)+d_1-\frac{d_3 c_1}{c_3}=0, \tag{21}$$

which is independent of the magnitude of non-linearity n_3, for $n_3 \neq 0$ because of the proportionality referred to above.

The corresponding amplitudes of the roll rate, p, and yaw rate, r, and the phase relationships with the translational velocity, $\bar{v}$, are given in the Appendix A.

It may also be shown that the discarded solution, i.e. $\Theta_3+\Theta_4 \neq 0$, given by equation (8), would lead to imaginary values of the frequency for the present example.

3.2. *Physical Implications.*

The advantage of an analytical approach such as the foregoing is that, in contrast to specific computer solutions, it provides a physical insight. For example, it is apparent from the approximate solutions (equations (12) and (19)) that the signs of the numerator and denominator define the type of motion which will arise in a particular case. A limit cycle can occur (i.e. Θ is real) only if numerator and denominator have the same sign, both expressions being determined at the steady flight angle of attack. The denominator, given approximately by

$$\frac{\partial R}{\partial \Theta^2} \approx \frac{3n_3}{4}\left(\frac{m}{\rho S s}\right)\left(\frac{\rho S V}{m}\right)^6 \left\{\left(\frac{l_p}{i_x}+\frac{n_r}{i_z}+y_v\right)\left(y_v+\frac{n_r}{i_z}\right)\left(\frac{l_p}{i_x}\right)^2+\frac{2n_r}{i_z}\cdot\frac{l_p}{i_x}\cdot y_v\left(y_v+\frac{n_r}{i_z}\right)+\right.$$

$$\left.+\frac{m}{\rho S s}\left[\frac{2n_r}{i_z}\cdot\frac{l_p}{i_x}\left(y_v+\frac{n_r}{i_z}\right)-\bar{w}\cdot\frac{l_v}{i_x}\left\{\left(\frac{n_r}{i_z}\right)^2+\left(\frac{l_p}{i_x}\right)^2+y_v\left(\frac{l_p}{i_x}+\frac{n_r}{i_z}\right)\right\}\right]\right\} . \tag{22}$$

can be shown to be positive throughout the range of angle of attack covered in the experiments (Fig. 3b). The numerator is Routh's discriminant, R, for the stability polynomial evaluated as if the non-linearities were absent, and for the HP 115 at low speeds this is shown in Fig. 3a. This changes sign at $\bar{w} = 0{\cdot}19$, so that for $\bar{w}$ below this value a normal convergent oscillation can be expected, and above, an oscillation will occur of a sustained amplitude which depends upon the magnitudes of $\frac{\partial R}{\partial(\Theta^2)}$ and R. The linear system is a degenerate case for which $\frac{\partial R}{\partial(\Theta^2)} = 0$, so that the motion is either convergent ($\Theta = 0$) or divergent ($\Theta = \infty$), depending only on the sign of R.

It will be noted from equation (22) that, because for the HP 115 the non-linearity is confined effectively to one term only, viz. the yawing moment, Θ^2 is inversely proportional to n_3.

The following two sections compare the predictions of this analytical method, firstly with experimental data (Section 3.3) and secondly with spot checks from digital computations (Section 3.4).

3.3. *Comparison with Experimental Values.*

3.3.1. *Damping index at small amplitudes.*

The responses obtained on the model of the HP 115 in the wind tunnel/flight dynamic simulator (Fig. 13c of Ref. 1) appear, at first sight, to be near zero damping at an angle of attack of 0·14, which is appreciably lower than the value of $\bar{w} \approx 0{\cdot}19$ given by the theory with non-linearities neglected. However, it is noticeable that the amplitude of $\bar{v}$ varies with the changes in $\bar{w}$ arising from a low frequency

cross-coupling oscillation, and so a simple approximate method of extracting the damping for a constant angle of attack is required. The theoretical value of the damping index (k), at small amplitudes where the non-linearity in $C_n(\bar{v})$ can be neglected, is almost linear with $\bar{w}$ (Fig. 4) so that the amplitude of the dutch roll oscillation was taken to be proportional to $e^{k(\bar{w})t}$, with $k(\bar{w})$ linear in $\bar{w}$. The logarithmic plot of the peaks of $\bar{v}$ could then be correlated with the variation of $\bar{w}$ in the experiments, to give k at mean values of $\bar{w}$.

Analysis of published[1] and unpublished records from the wind tunnel/flight dynamic simulator shows that zero damping occurs at about $\bar{w} = 0{\cdot}195$, and that theoretical and experimental values of damping index agree well (Fig. 4).

3.3.2. *Amplitude and frequency of the steady oscillation.*

A detailed examination of the apparently steady amplitude oscillations in Ref. 1 and unpublished results showed that the amplitude was still increasing very slightly because of the finite duration of the tunnel tests. Before comparing the steady state amplitudes with the theoretical predictions it was therefore necessary to extrapolate the measured values to the true terminal values.

A method of predicting the amplitude growth rate was needed, and a more general solution to equation (13) was developed, again from the method in Section 2 but without the constraint of $\lambda \equiv 0$. The intermediate amplitude during the growth to the asymptotic value, Θ, is denoted here by θ. For the particular form of the non-linearity assumed, viz. $C_n = n_1 \bar{v} + n_3 \bar{v}^3$, the equations corresponding to equations (9) and (10) are:

$$\omega^2\left\{a_1+\frac{3a_3}{4}\theta^2+4\lambda\right\} = c_1+\tfrac{3}{4}c_3\theta^2+2\lambda(b_1+\tfrac{9}{4}b_3\theta^2)+3\lambda^2(a_1+\tfrac{27}{4}a_3\theta^2)+4\lambda^3 \tag{23}$$

$$\omega^4-\omega^2\{b_1+\tfrac{3}{4}b_3\theta^2+3\lambda(a_1+\tfrac{9}{4}a_3\theta^2)+6\lambda^2\}-\{d_1+\tfrac{3}{4}d_3\theta^2+\lambda(c_1+\tfrac{9}{4}c_3\theta^2)+$$

$$+\lambda^2(b_1+\tfrac{27}{4}b_3\theta^2)+\lambda^3(a_1+\tfrac{81}{4}a_3\theta^2)+\lambda^4\} = 0. \tag{24}$$

These yield a sextic relating λ and θ^2 which for the parameters appropriate to the HP 115 aircraft may be approximated by a quadratic in λ. The relationship between λ and θ^2 is shown in Fig. 5a where the results for different angles of attack are collapsed by plotting λ/λ_0 against θ^2/Θ^2, λ_0 being the damping at zero amplitude ($\lambda_0 \equiv -k$). From this the time, τ, for the amplitude to grow from θ_1 to θ_2

$$\left(\equiv \int_{\theta_1}^{\theta_2} \frac{\mathrm{d}\theta}{\dot{\lambda}\theta}\right) \tag{25}$$

may be determined by numerical integration, as shown in Fig. 5b, where it is compared with a computer solution (Section 3.4).

In Ref. 2 it was shown that the present technique gives for the limit cycle appropriate to the van der Pol equation a variation in λ of

$$\lambda = \lambda_0\left[1-\left(\frac{\theta}{\Theta}\right)^2\right]. \tag{26}$$

This much simpler relationship between λ and θ^2 has also been plotted in Fig. 5a where it is seen to be in remarkably close agreement with the present solution. It has the advantage that when inserted in equation (25), τ is obtained in a closed form, viz.

$$\tau = \frac{1}{2\lambda_0}\log\left[\frac{\theta_2^2(\Theta^2-\theta_1^2)}{\theta_1^2(\Theta^2-\theta_2^2)}\right]. \tag{27}$$

This is also plotted in Fig. 5b, showing it to be a close approximation to the present formal solution. But it also has the important advantage that it enables the steady state amplitude to be specified in terms of points on the growth curve, in particular the point of inflection, θ_i. For this simple variation of λ with θ,

$$\Theta = \sqrt{3}\,\theta_i\,. \tag{28}$$

When checked against the formal theoretical solution (Fig. 6) this is found to apply equally, and hence it provides the necessary means for extrapolating the experimental results (Fig. 7).

This study of the growth rate to the final limit cycle amplitude is useful and interesting in its own right, but since it is required here only for this extrapolation, it has not been pursued further.

The estimated experimental values of the steady amplitude Θ, although significantly larger than the maximum values during the tests, are still smaller than the theoretical values, although the character of the variation with $\bar{w}$ is similar, as shown in Fig. 8. Reducing the range of $\bar{v}$ over which C_n is fitted tends to decrease the theoretical value of Θ, but not sufficiently to give good agreement. However, there are a number of possible causes of disagreement, which can affect the fine balance on which the amplitude clearly depends, and it is encouraging to find that the theory predicts the character of the response as closely as it does. The effects of changing the representation of $C_n(\bar{v})$ are discussed further in section 4. It is also noticeable that the departure of $C_y(\bar{v})$ from the assumed linear variation is in the correct sense to reduce the theoretical value of Θ, and hence to reduce the discrepancy, but it was not thought worthwhile to evaluate the more complicated algebraic expressions which arise.

The frequency of the oscillations at large amplitude could be determined from the experimental responses directly, and good agreement is obtained between theoretical and experimental values, as shown in Fig. 8b. It is interesting to note that the increase in frequency due to the non-linear C_n, predicted by theory (see Fig. 10 for example) does occur.

One of the experiments described in Ref. 1 was undertaken to examine the effect of reduction in the value of the rolling moment due to sideslip, and so corresponding calculations were made, the results being shown in Fig. 9. The mean angles of attack for the three tests were 0·25, 0·255 and 0·245 for the 100 per cent, 90 per cent and 75 per cent of $C_l(\bar{v})$ respectively, so a mean value of $\bar{w} = 0{\cdot}25$ was assumed for the theoretical calculations. Again, the frequency agrees well, but the theoretical amplitude is about twice that indicated in the experiment, although the general trend is correct.

3.4. *Digital Solution.*

In order to check the present theory with an 'exact' solution, the equations of motion, equations (13), were solved numerically for specific cases, using available subroutines to perform the integrations on the ICL 1907 digital computer. The resulting amplitudes and frequencies at $\bar{w} = 0{\cdot}225$ and 0·25 are shown in Fig. 10, and are seen to be almost identical to the values given by equations (11) and (19). Similar good agreement was obtained for the amplitudes of the oscillations in rates of roll and yaw, and for the phases between the responses. The formulae, in terms of Θ and ω are given in Appendix A, together with a comparison of the results.

The digital computations also demonstrated that the steady oscillation is a true limit cycle for the constrained flight condition with constant angle of attack, in that an initial disturbance greater in magnitude than the steady value converged to the steady value. The peak values of the responses in $\bar{v}$ and p have been plotted in Fig. 11, as a function of peak number after the initial disturbance, for various initial conditions.

The general agreement between the exact (i.e. digital computer) solutions and the approximate analytic solutions is very encouraging, and gives confidence in the extension of the method of Ref. 2 to higher order systems, at least in the case where only one sustained oscillatory mode is present.

4. *Representation of Yawing Moment Due to Sideslip.*

In the foregoing the representation of the non-linearity in the yawing moment of HP 115 has been

confined to a cubic term. The form of the solutions obtained suggest that the balance, particularly in the amplitude of the sustained oscillation (which, but for the non-linearity, would tend to become infinite, Section 3.2) might be rather fine and depend critically on the form assumed for the non-linearity. It was therefore decided to investigate this further for the representations in the following sections.

4.1. *Representation by Two Straight Lines.*

The experimental values of yawing moment due to sideslip were approximated by two straight lines, that is n_v is assumed to change value at a particular angle of sideslip. This type of representation is often more convenient than a continuous functional dependence in computer studies, and has been used in many flight simulators. The resulting equations of motion may be treated in a similar way to that for the functional dependence described in Section 2, and the use of the technique for equations with discontinuous coefficients has been confirmed by comparison with exact results for a second order equation in Appendix B.

For the HP 115 aircraft, we write

$$\begin{aligned} C_n(\bar{v}) &= n_{v_1}\,\bar{v} \qquad \text{for } 0 < |\bar{v}| < \bar{v}_1\,, \\ C_n(\bar{v}) &= n_{v_2}\,\bar{v}+\gamma_1 \quad \text{for } \bar{v} > \bar{v}_1 \\ \text{and} \qquad C_n(\bar{v}) &= n_{v_2}\,\bar{v}-\gamma_1 \quad \text{for } \bar{v} < -\bar{v}_1 \end{aligned} \tag{29}$$

where $\gamma_1 = (n_{v_1}-n_{v_2})\,\bar{v}_1$ for continuity at $\bar{v} = \pm\bar{v}_1$. The equations of motion then reduce to a fourth order differential equation with coefficients $A(\bar{v}) \ldots D(\bar{v})$ linear in $\bar{v}$, but discontinuous at $\bar{v} = \pm\bar{v}_1$, and with one additional constant term if $|\bar{v}| > \bar{v}_1$.

For the approximate solution, we again write

$$\bar{v} = \Theta \cos\phi\,, \text{ with } \bar{v}_1 = \Theta\cos\phi_1\,, \tag{30}$$

and integration over one cycle of ϕ gives finally that

$$a_{11}\,\omega^2 = c_{11}+(c_{12}-c_{11})\,(2\phi_1-\sin 2\phi_1)/\pi \tag{31}$$

and

$$\omega^4-b_{11}\,\omega^2+d_{11} = \frac{1}{\pi}\left[\omega^2\,(b_{12}-b_{11})\,(2\phi_1+\sin 2\phi_1)-(d_{12}-d_{11})\,(2\phi_1-\sin 2\phi_1)\right] \tag{32}$$

The coefficients $a_{11} \ldots d_{11}$ are given by the expression for $a_1 \ldots d_1$ in equations (14) to (17) with $n_1 = n_{v_1}$, and similarly $a_{12} \ldots d_{12}$ with $n_1 = n_{v_2}$.

At a given angle of attack, the equations of motion are linear when $|\bar{v}| < v_1$, and so the dutch roll oscillation is convergent or divergent according as Routh's discriminant for the coefficients $a_{11} \ldots d_{11}$ is positive or negative. If $R(n_{v_1}) > 0$, it is found that equations (31) and (32) have no solution, as would be expected for a damped oscillation, but as the angle of attack is increased the condition for neutral stability, $R(n_{v_1}) = 0$, is reached, and equations (31) and (32) give $\phi_1 = 0$. At the angle of attack corresponding to $R = 0$ the response from the linear equations of motion would be a sustained oscillation with amplitude dependent on the initial conditions, but if the initial value of $\bar{v}$ is greater than $\bar{v}_1$, then the non-linear contribution fixes the amplitude at $\Theta = \bar{v}_1$. This contrasts with the solution for the cubic representation of C_n where the amplitude of the sustained oscillation is zero at a similar angle of attack.

As the angle of attack is increased further, $R(n_{v_1})$ becomes increasingly negative, and if $R(n_{v_2})$ remains positive, equations (31) and (32) give one solution for ϕ_1 in the acceptable range $0 \leqslant \phi_1 \leqslant \pi/2$, and so the variation of Θ with $\bar{w}$ may be obtained. However, $R(n_{v_2})$ may also become negative as the angle of attack is increased further, and then either two or no solutions for ϕ_1 exist, dependent on the magnitude of $|R(n_{v_2})|$.

In physical terms, if the inner portion of the oscillation ($|\bar{v}| \leqslant \bar{v}_1$) is stable the kinetic energy will be dissipated and there will be no sustained oscillation. If this inner portion is neutrally stable, ($R(n_{v_1}) = 0$) there will be no loss of kinetic energy for $|\bar{v}| \leqslant \bar{v}_1$, but the positive damping outside this range will result in a sustained oscillation of amplitude v_1. If the inner portion is unstable, kinetic energy will be acquired in traversing the range $\pm\bar{v}_1$, which in the equilibrium state will be dissipated by the positively damped outer portion. The sustained oscillation amplitude will thus be greater than v_1.

For the HP 115 aircraft, the range of angle of attack for which one solution of the equations exists is $0{\cdot}194 < \bar{w} < 0{\cdot}221$, the values of n_{v_1}, n_{v_2} and $\bar{v}_1$ being obtained using a least-squares fitting technique on the experimental data for $C_n(\bar{v})$. The results for Θ and ω are shown in Fig. 12, together with the experimental values. In the range $0{\cdot}221 < \bar{w} = 0{\cdot}234$, two values of Θ exist and for $\bar{w} > 0{\cdot}234$, theory gives no possible solutions for a sustained oscillation.

Numerical integration of the equations of motion confirms the predicted amplitudes and frequency. Thus it appears that the representation of $C_n(\bar{v})$ by two straight lines could lead to responses of quite a different character from those obtained using a continuously varying function. In addition, of course, the responses have discontinuities in slope at $\bar{v} = \bar{v}_1$, which are not present in a more complete simulation of the motion.

4.2. *Higher order Polynomial Representation.*

Because of this sensitivity to the form of the non-linearity, some alternative representations of $C_n(\bar{v})$ were considered briefly.

The experimental data for $C_n(\bar{v})$ does exhibit some scatter about the mean cubic representation (see Fig. 1), and so a quintic term was also considered, viz

$$C_n = n_1\,\bar{v} + n_3\,\bar{v}^3 + n_5\,\bar{v}^5\,. \tag{33}$$

The coefficients n_1, n_3 and n_5 were again obtained by a least-squares fitting technique using experimental values of C_n for $\bar{v} \leqslant 0{\cdot}15$ for each $\bar{w}$, but the extrapolation of C_n up to the amplitudes given by equation (11) led to an unrealistic variation of C_n with $\bar{v}$, negative values of $\partial C_n/\partial\bar{v}$ occurring.

The simpler quintic representation of C_n by $n_1\,\bar{v} + n_5\,\bar{v}^5$ avoids such difficulties, and leads to smaller values of Θ (at the larger angles of attack) than the cubic representation of C_n, see Fig. 13, but they are still larger than the experimental values. The frequencies are almost identical for both representations, because the values of n_1 are not very different. Since the theoretical values of Θ are beyond the range of $\bar{v}$ for which C_n was fitted, it is necessary to consider the extrapolated values of C_n up to $\bar{v} = \Theta$. A comparison between the cubic and the simple quintic representations of C_n, and the experimental data, is given in Fig. 13b for $\bar{w} = 0{\cdot}25$. It may be seen that neither extrapolation agrees with the measured value of C_n at $\bar{v} = 0{\cdot}175$, but it does not seem worthwhile to search for alternative polynomials which would give perfect quantitative agreement between experimental and theoretical values of Θ.

It is clear that the predicted amplitude of the sustained oscillation is sensitive to the analytic form assumed for the non-linearity, and that it is important to be able to define this reliably over the amplitude of the oscillation.

5. *Conclusions.*

(1) An extension of the analytical method of Ref. 2 to the treatment of fourth order, non-linear systems has been shown to predict very closely the conditions in which sustained oscillations were obtained in the dutch roll motion of the HP 115 aircraft.

(2) The approximation method has been checked against solutions from a digital computation of the full non-linear differential equations and found to give convincing agreement. The analytical form of the approximation, however, has the advantage of giving insight into the physical nature of the problem, and shows, for example, that the criterion for the eixstence of such sustained oscillations is a non-linear analogue of Routh's stability discriminant.

(3) Non-linearity with sideslip of one parameter—n_v—accounts qualitatively and quantitatively for the

behaviour. The incidence for the onset of the sustained oscillations is predicted together with the variation of frequency as the incidence is further increased to values at which, but for the non-linearity, the motion would be divergent. There is, however, some disparity between the predicted and experimental amplitudes in this condition.

(4) There is evidence that for conventional simulations some care is needed in the representation of the non-linear aerodynamic terms if this type of essentially non-linear dynamic motion is to be reproduced. The customary representation by a series of straight lines may be inadequate.

(5) Inasmuch as the wind tunnel (FDS) technique has reproduced the flight behaviour, and the present analytical approach has produced good agreement with the experimental data, the relevance and accuracy of the wind tunnel simulation technique is regarded as having been fully demonstrated.

LIST OF SYMBOLS

$A(x)$, $B(x)$, $C(x)$, $D(x)$	Polynomials in basic differential equation (1)
a_n	Coefficient of x^n in $A(x)$
b_n	Coefficient of x^n in $B(x)$
c_n	Coefficient of x^n in $C(x)$
d_n	Coefficient of x^n in $D(x)$
C_l	Rolling moment coefficient, $\mathscr{L}/\rho V^2 Ss$
C_n	Yawing moment coefficient, $\mathscr{N}/\rho V^2 Ss$
C_y	Sideforce coefficient, $Y/\frac{1}{2}\rho V^2 S$
C_z	Normal force coefficient, $\mathscr{Z}/\frac{1}{2}\rho V^2 S$
e_x	Product of inertia ratio, $-I_{zx}/I_x$
e_z	Product of inertia ratio, $-I_{zx}/I_z$
$F(x, \dot{x})$	Function in differential equation, Section 2
g	Acceleration due to gravity
I_x	Moment of inertia in roll
I_z	Moment of inertia in yaw
I_{zx}	Product of inertia
i_x	Normalised moment of inertia, I_x/ms^2
i_z	Normalised moment of inertia, I_z/ms^2
K_1, K_2, K_3	Functions used in Section 2
k	Damping index

$-k_1, k_2$	Damping indices for second order systems, Appendix B
$\mathscr{L}$	Rolling moment
l_v	Rolling moment derivative due to sideslip, $\frac{1}{\rho V^2 Ss}\frac{\partial \mathscr{L}}{\partial \bar{v}}$
l_p	Rolling moment derivative due to rate of roll, $\frac{1}{\rho SVs^2}\frac{\partial \mathscr{L}}{\partial p}$
l_r	Rolling moment derivative due to rate of yaw, $\frac{1}{\rho SVs^2}\frac{\partial \mathscr{L}}{\partial r}$
m	Mass of aircraft
$\mathscr{N}$	Yawing moment
n_p	Yawing moment derivative due to rate of roll, $\frac{1}{\rho SVs^2}\frac{\partial \mathscr{N}}{\partial p}$
n_r	Yawing moment derivative due to rate of yaw, $\frac{1}{\rho SVs^2}\frac{\partial \mathscr{N}}{\partial r}$
n_{v_1}, n_{v_2}	Slopes of $C_n(\bar{v})$ in straight line representation
n_1, n_3, n_5	Coefficients of $\bar{v}$, $\bar{v}^3$, $\bar{v}^5$ respectively in polynomial representation of $C_n(\bar{v})$
p	Rate of roll
r	Rate of yaw
R	Routh's discriminant
R_m	Residual term associated with $\frac{d^m}{dt^m}$, defined in Section 2
S	Wing area
s	Wing semi-span
t	Time
V	Forward velocity
$\bar{v}$	Sideslip velocity/V, (angle of sideslip)
$\bar{w}$	Normal velocity/V, (angle of attack)
x	Variable in basic differential equation
x_1	Particular value of x, Appendix B
$X(n)$	Coefficient defined after equation (10), $X(n) = \frac{(2n+1)!}{2^{2n}\, n!\,(n+1)!}$
Y	Sideforce
Z	$\lambda + {}^{i}\omega$

y_p	Sideforce coefficient due to rate of roll, $\frac{1}{\rho SVs}\frac{\partial Y}{\partial p}$
y_r	Sideforce coefficient due to rate of yaw, $\frac{1}{\rho SVs}\frac{\partial Y}{\partial r}$
y_v	Sideforce coefficient due to rate of sideslip, $\frac{1}{\rho SV^2}\frac{\partial Y}{\partial \bar{v}}$
Z	Normal force
γ_1	Particular value of $\bar{v}$ defined in equation (29)
ε_p	Phase angle of p relative to $\bar{v}$
ε_r	Phase angle of r relative to $\bar{v}$
θ	Amplitude of $\bar{v}$
θ_i	Amplitude of $\bar{v}$ at point of inflection of $\theta(t)$
$\theta_1, \theta_3, \theta_4$	Amplitudes of various possible modes of $\bar{v}$
Θ	Amplitude of steady oscillation in $\bar{v}$
Θ_p	Amplitude of steady oscillation in p
Θ_r	Amplitude of steady oscillation in r
λ	$\dot{\theta}\,\theta$ (Section 3.3.2)
λ_o	Value of λ at zero amplitude (Section 2)
λ_n	$= \dot{\theta}_n/\theta_n$ (Section 2)
ρ	Air density
τ	Time for amplitude growth
φ	Bank angle
ϕ	Defined in equation (5)
ϕ_1	Particular value of ϕ, Section 4.1
ω	$= \dot{\phi}$, equivalent to frequency
ω_1, ω_2	Undamped frequencies of second order systems, Appendix B
ν_1, ν_2	Frequencies of second order systems, Appendix B
Superscript	
*	Equivalent value

LIST OF REFERENCES

No.	*Author(s)*	*Title, etc.*
1	D. W. Partridge and B. E. Pecover	An application of the R.A.E. wind-tunnel/flight dynamics simulator to the low-speed dynamics of a slender delta aircraft (HP 115). A.R.C. R. & M. 3669 (1969).
2	L. J. Beecham and I. M. Titchener	Some notes on an approximate solution for the free oscillation characteristics of non-linear systems typified by $\ddot{x}+F(x,\dot{x})=0$. A.R.C. R. & M. 3651 (1969).

APPENDIX A

Amplitudes and Phase Angles of Rates of Roll and Yaw.

Analogous expressions for roll rate and yaw rate may be used in equations (13) to that defined for sideslip velocity in equation (5), and they may be written as

$$p = \Theta_p \cos(\phi+\varepsilon_p)$$
$$r = \Theta_r \cos(\phi+\varepsilon_r)$$

where $\bar{v} = \Theta\cos\phi$.
The values of Θ_p etc. are obtained by substitution of $\bar{v}$ into the first two equations of (13), to give:

$$\Theta_p = \frac{\Theta}{(1-e_x e_z)} \cdot \frac{n_3}{si_x i_z}\left(\frac{\rho SV}{m}\right)^4 \left[\frac{\hat{\omega}^4 k_r^2+\hat{\omega}^2(i_{xz}\hat{\omega}^2+j_r)^2}{(b_3\omega^2-d_3)^2+c_3^2\omega^2}\right]^{\frac{1}{2}}$$

$$\Theta_r = \frac{\Theta}{(1-e_x e_z)} \cdot \frac{n_3}{si_x i_z}\left(\frac{\rho SV}{m}\right)^4 \left[\frac{(k_p\hat{\omega}^2-k)^2+\hat{\omega}^2(i_x\hat{\omega}^2-j_p)^2}{(b_3\omega^2-d_3)^2+c_3^2\omega^2}\right]^{\frac{1}{2}}$$

$$\tan\varepsilon_p = \frac{1}{\hat{\omega}}\left[\frac{\frac{m}{\rho SV}(\omega^2 b_3-d_3)(i_{xz}\hat{\omega}^2+j_r)+\omega^2 c_3 k_r}{\frac{m}{\rho SV}(\omega^2 b_3-d_3)k_r-c_3(i_{xz}\hat{\omega}^2+j_r)}\right]$$

$$\tan\varepsilon_r = \hat{\omega}\left[\frac{c_3(\hat{\omega}^2 k_p-k)-\frac{m}{\rho SV}(\omega^2 b_3-d_3)(i_x\hat{\omega}^2+j_p)}{\hat{\omega}^2 c_3(i_x\hat{\omega}^2+j_p)+\frac{m}{\rho SV}(\omega^2 b_3-d_3)(\hat{\omega}^2 k_p-k)}\right]$$

where the following symbols have been introduced,

$$k_r = l_r - i_{xz} y_v, \quad k_p = l_p + i_x y_v$$

$$j_r = \frac{m}{\rho Ss} l_v + y_v l_r - y_r l_v$$

$$j_p = \frac{m}{\rho Ss} l_v \bar{w} + y_p l_v - l_p y_v$$

$$k = \frac{m}{\rho Ss} \frac{C_z}{2} l_v$$

$$\hat{\omega} = \frac{m}{\rho SV} \omega$$

The numerical results obtained for $\bar{w} = 0{\cdot}225$ are compared in the table below with the values obtained for the numerical integration of the equations of motion,

	Θ_p	Θ_r	ε_p	ε_r
Equations	0·047	0·0021	−68·7°	47·2°
Numerical integration	0·047	0·0023	−69°	42°

APPENDIX B

Second Order System with Discontinuous Coefficients.

The validity of using the approximate method for equations with discontinuous coefficients has also been checked by solving the piece-wise linear equations analytically rather than numerically. In order to reduce the algebra, a second order system has been considered, which is similar to the oscillatory mode of the fourth order system analysed in the main part of this Report, i.e.

$$\ddot{x} + \frac{d\,A(x)}{dt} + B(x) = 0 \tag{B.1}$$

where $0 < |x| < x_1, A(x) = -2k_1 x, B(x) = \omega_1^2 x$

$$x > x_1, A(x) = 2k^2 x - x_1 (2k_2 - 2k_1), B(x) = \omega_2^2 x - x_1 (\omega_2^2 - \omega_1^2)$$

$$x < -x_1, A(x) = 2k_2 x + x_1 (2k_2 - 2k_1), B(x) = \omega_2^2 x + x_1 (\omega_2^2 - \omega_1^2)$$

and k_1 and k_2 are both positive.

The solutions in the time intervals, illustrated in Fig. 14a, $t_1 < t < t_2$ when $x > x_1$, $t_2 < t < t_3$ when $|x| < x_1$, $t_3 < t < t_4$ when $x < -x_1$, and $t_4 < t < t_5$ when $|x| < x_1$, may be obtained in terms of the value of $\dot{x}\,(= \dot{x}_1$ say) at $t = t_1$, with the solutions matched at $t = t_2, t_3, \ldots$ The condition for a steady oscillation to exist is that $\dot{x}_1 = -\dot{x}_3\,(= \dot{x}_5)$, and this is sufficient to determine the time intervals $t_2 - t_1$ $(= t_4 - t_3)$ and $t_3 - t_2\,(= t_5 - t_4)$, and also the value of $\dot{x}_1$.

The condition for a continuous value of $\dot{x}$ at $t = t_2$ gives that

$$\frac{\dot{x}_2}{x_1} = \frac{\omega_1^2}{\omega_2^2}\left\{\frac{v_2}{\sin v_2(t_2-t_1)}[\cos v_2(t_2-t_1) - e^{-k_2(t_2-t_1)}] - k_2\right\}$$

$$= k_1 - \frac{v_1}{\sin v_1(t_3-t_2)}[\cos v_1(t_3-t_2) + e^{-k_1(t_3-t_2)}] \tag{B.2}$$

and for $\dot{x}_1 = -\dot{x}_3$, then

$$\frac{\dot{x}_1}{x_1} = \frac{\omega_1^2}{\omega_2^2}\left\{\frac{v_2}{\sin v_2(t_2-t_1)}[e^{k_2(t_2-t_1)} - \cos v_2(t_2-t_1)] - k_2\right\}$$

$$= k_1 + \frac{1}{\sin v_1(t_3-t_2)}e^{k_1(t_3-t_2)} + \cos v_1(t_3-t_2) \tag{B.3}$$

where $\omega_1^2 = v_1^2 + k_1^2$ and $\omega_2^2 = v_2^2 + k_2^2$. (B.4)

These may be solved graphically for $v_2(t_2-t_1)$ and $v_1(t_3-t_2)$ in terms of the parameters k_1/v_1, k_2/v_2 and k_1/k_2.

The amplitude of the steady oscillation is given by

$$\frac{\Theta}{x_1} = 1 + \frac{\omega_1^2}{\omega_2^2}\left\{\frac{v_2}{\omega_2 \sin v_2(t_2-t_1)}[1 - 2e^{k_2(t_2-t_1)}\cos v_2(t_2-t_1) + e^{2k_2(t_2-t_1)}]^{\frac{1}{2}} e^{-k_2(T_1-t_1)} - 1\right\} \tag{B.5}$$

where

$$\tan v_2(T_1-t_1) = \frac{v_2[e^{k_2(t_2-t_1)} - \cos v_2(t_2-t_1)] - k_2 \sin v_2(t_2-t_1)}{v_2 \sin v_2(t_2-t_1) + k_2[e^{k_2(t_2-t_1)} - \cos v_2(t_2-t_1)]} \tag{B.6}$$

and the frequency of the oscillation may be written as

$$\omega = \pi/[(t_2-t_1) + (t_3-t_2)]. \tag{B.7}$$

These equations (B.5) to (B.7) may be arranged to give $\frac{\Theta}{x_1}$ and $\frac{\omega}{k_2}$ in terms of k_1/v_1, k_2/v_2 and k_1/k_2.

The approximate solution for the amplitude and frequency of the steady oscillation has been obtained by assuming that $x = \Theta \cos \phi$, with $\dot{\Theta} = 0$ and $\dot{\phi} = \omega$. If $\cos \phi_1 = x_1/\Theta$, then the integrations over one cycle give that

$$\Theta = x_1 \sec \phi_1 \quad \text{where} \quad 2\phi_1 - \sin 2\phi_1 = \pi k_1/(k_1+k_2) \tag{B.8}$$

and

$$\omega^2 = (k_2\omega_1^2 + k_1\omega_2^2)/(k_1+k_2). \tag{B.9}$$

The exact and approximate values of amplitude and frequency, expressed as Θ/x_1 and ω/k_2, are shown in Figs. 14b and c for the two general cases (i) $k_1/v_1 = 0{\cdot}1$, $k_2/v_2 = 0{\cdot}2$ and (ii) $k_1/v_1 = k_2/v_2 = 1{\cdot}0$, over the range of k_1/k_2 from 0 to ∞, and for a particular case, close to the frequencies and dampings associated with the HP 115, $\omega_1^2 = 6{\cdot}5$, $\omega_2^2 = 7{\cdot}0$ and $k_2 = 0{\cdot}05$ for varying k_1. The exact values of the amplitudes for all cases collapse on to the one approximate curve, which depends only on k_1/k_2, with

small errors arising as $k_2/k_1 \to 0$ when $\Theta \to \infty$. The frequencies also agree remarkably well, even for the large damping factors of 1·0.

It is also possible to show that the exact solution tends towards the steady oscillation when started from an arbitrary initial condition, by considering the relationships between the values of $\dot{x}$ at $x = +x_1$ and $x = -x_1$ throughout the transient response.

TABLE

Numerical Values Used In Calculations.

Mass and inertias

m	2154 kg
i_x	0·109
i_z	1·27
i_{xz}	0·0806

Representative length $s = 3{\cdot}05$ m

Representative area $S = 40{\cdot}18$ m^2

Air density $\rho = 0{\cdot}906$ kg/m^3

Derivatives due to rate of roll and rate of yaw

$$y_p = 0{\cdot}014 + 0{\cdot}505\,\bar{w} - 0{\cdot}474\,\bar{w}^2$$

$$l_p = -0{\cdot}132 + 0{\cdot}08\,\bar{w}$$

$$n_p = 0{\cdot}0125\,\bar{w} - 0{\cdot}938\,\bar{w}^2$$

$$y_r = 0$$

$$l_r = 0{\cdot}006 + 0{\cdot}54\,\bar{w}$$

$$n_r = -0{\cdot}351 - 0{\cdot}089\,\bar{w}$$

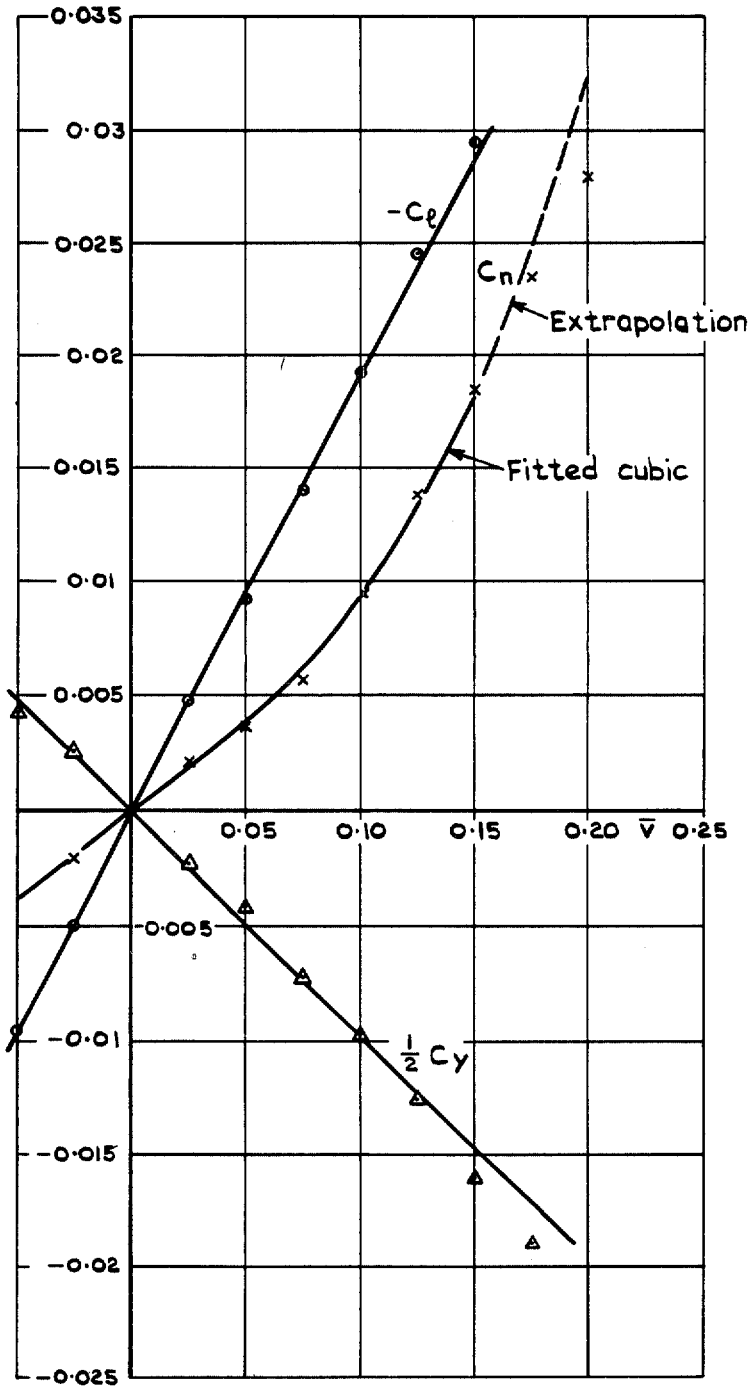

FIG. 1. Approximations to C_y, C_l and C_n at $\bar{w} = 0{\cdot}25$.

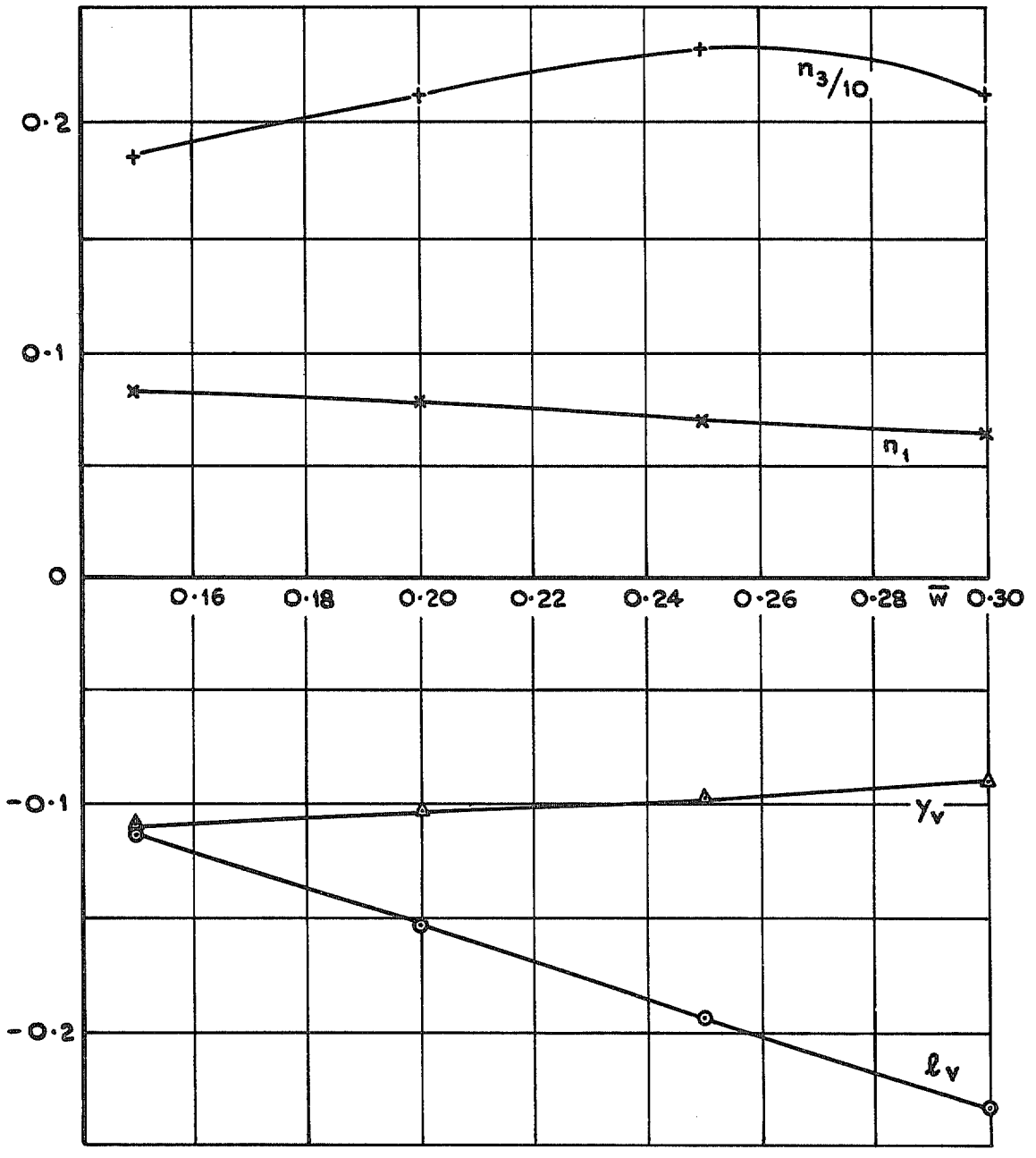

FIG. 2. Variation with angle of attack of sideslip derivatives, l_v and y_v, and coefficients in cubic representation of $C_n(\bar{v}) = n_1 \bar{v} + n_3 \bar{v}^3$ (HP 115 aircraft model).

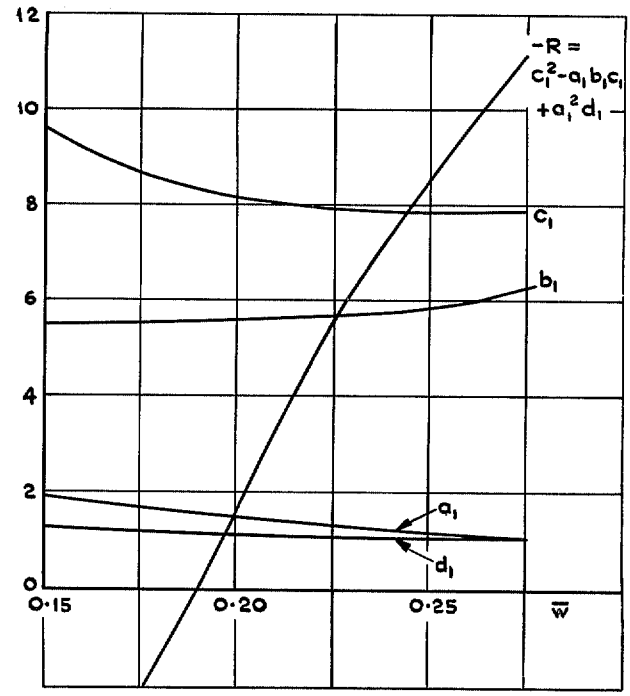

a Coefficients of linear terms of polynomials, and Routh's discriminant

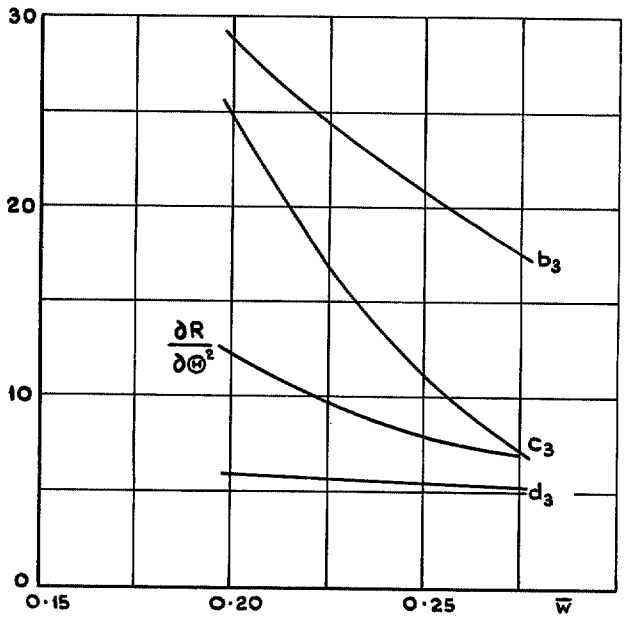

b Coefficients of cubic terms of polynomials, and parameter $\frac{\partial R}{\partial \Theta^2}$

FIG. 3a & b. Coefficients applicable to HP 115.

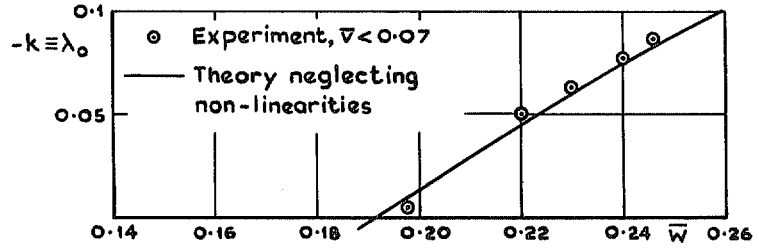

FIG. 4. Comparison of experimental and theoretical values of damping at small amplitudes.

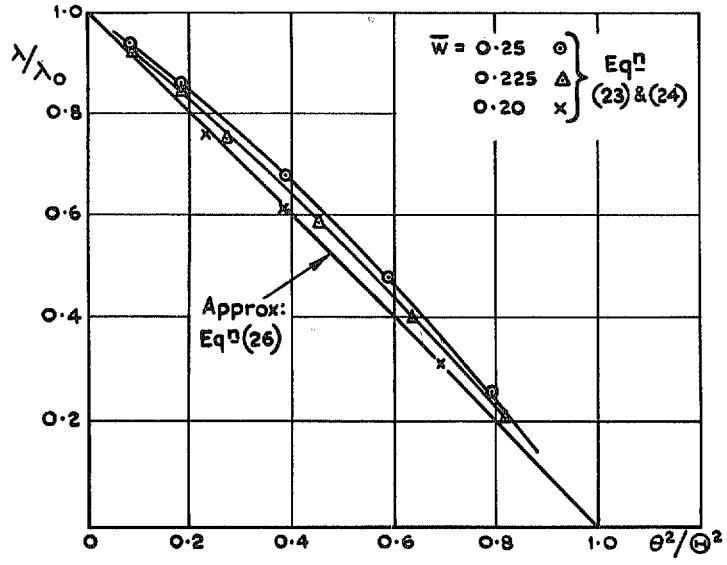

a Variation of damping with amplitude

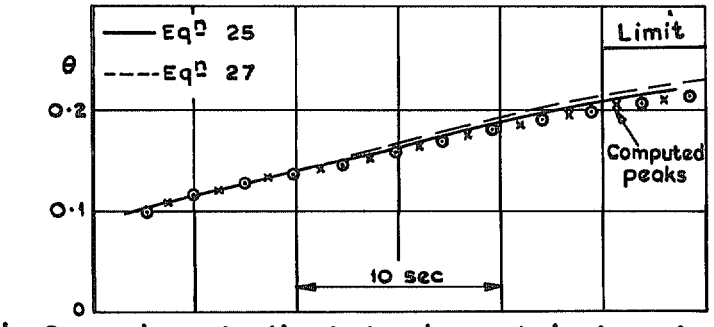

b Comparison of estimated and computed values of amplitude variation with time

FIG. 5a & b. Computed and approximate variation of damping and amplitude.

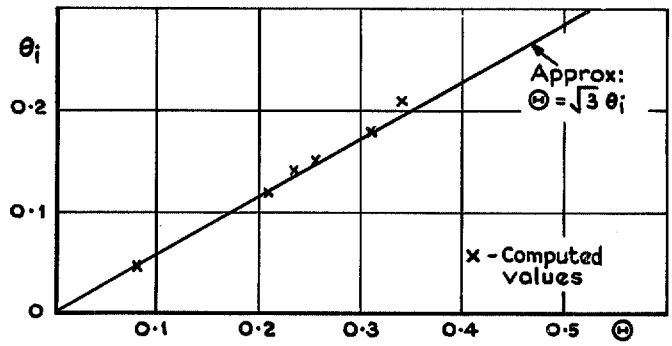

FIG. 6. Relation between amplitudes at inflection point and steady value.

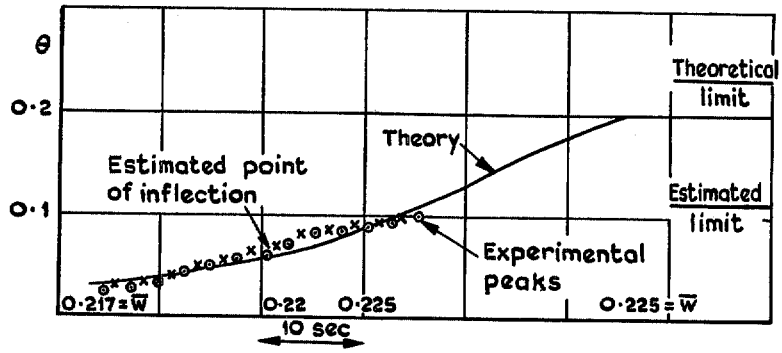

a Comparison with Fig.13e of Ref 1

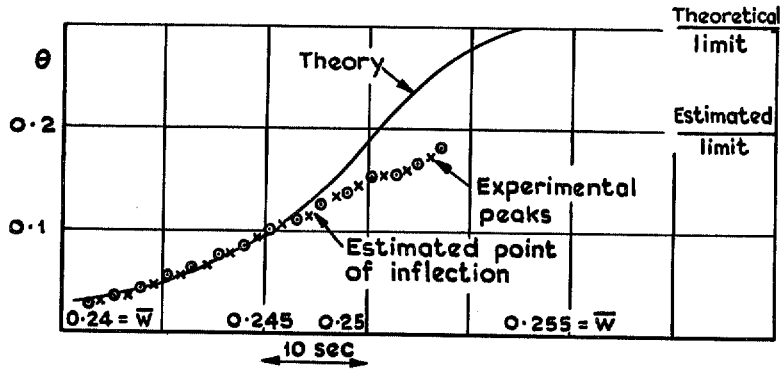

b Comparison with Fig.13g of Ref 1

FIG. 7a & b. Theoretical and experimental envelopes of response in $\bar{v}$.

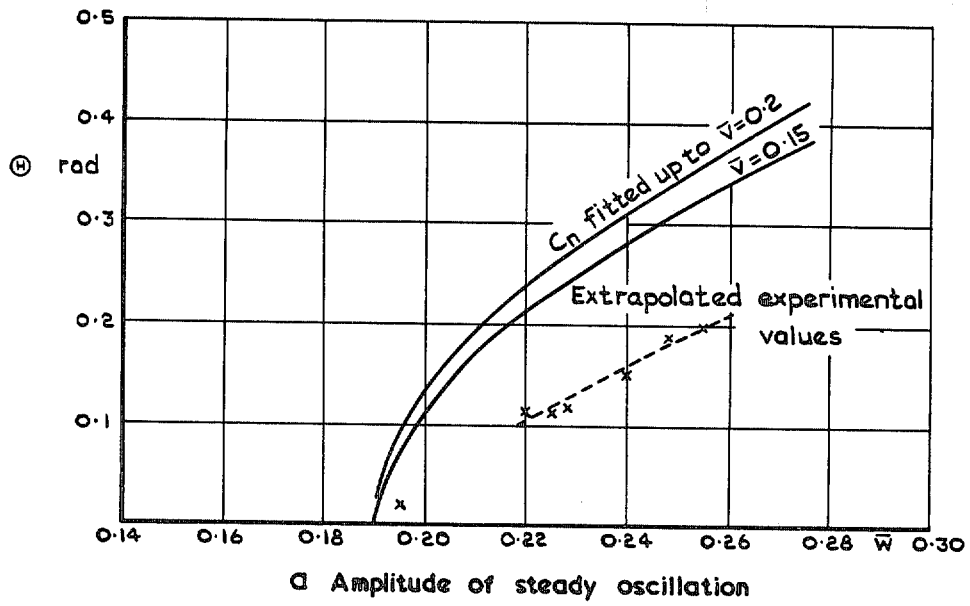

a Amplitude of steady oscillation

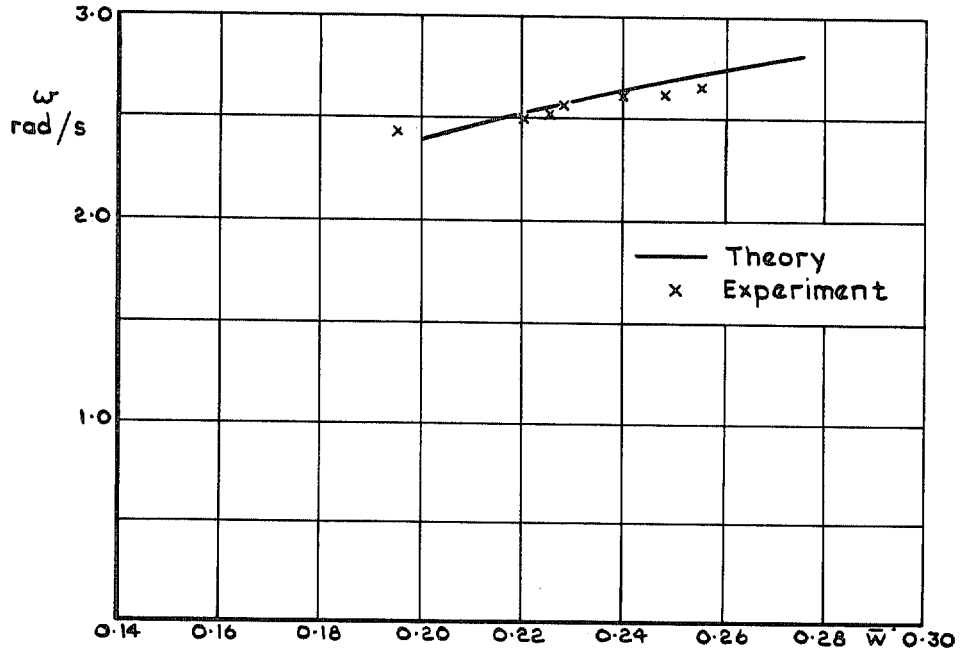

b Frequency of steady oscillation

FIG. 8a & b. Comparison between experimental and theoretical values of amplitude and frequency (HP 115 aircraft model).

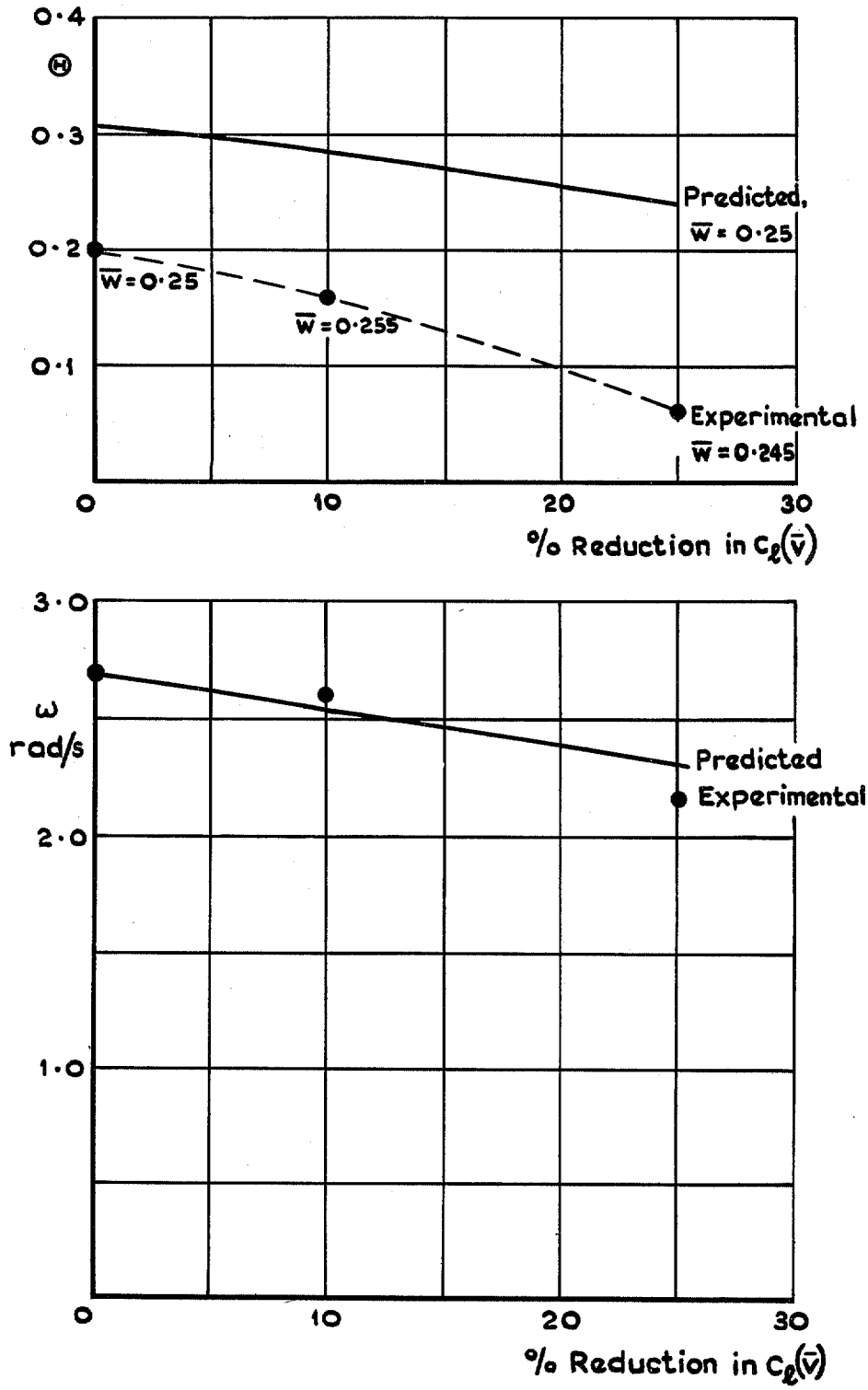

FIG. 9. Experimental and theoretical effects of reducing $C_l(\bar{v})$, at $\bar{w} \approx 0{\cdot}25$.

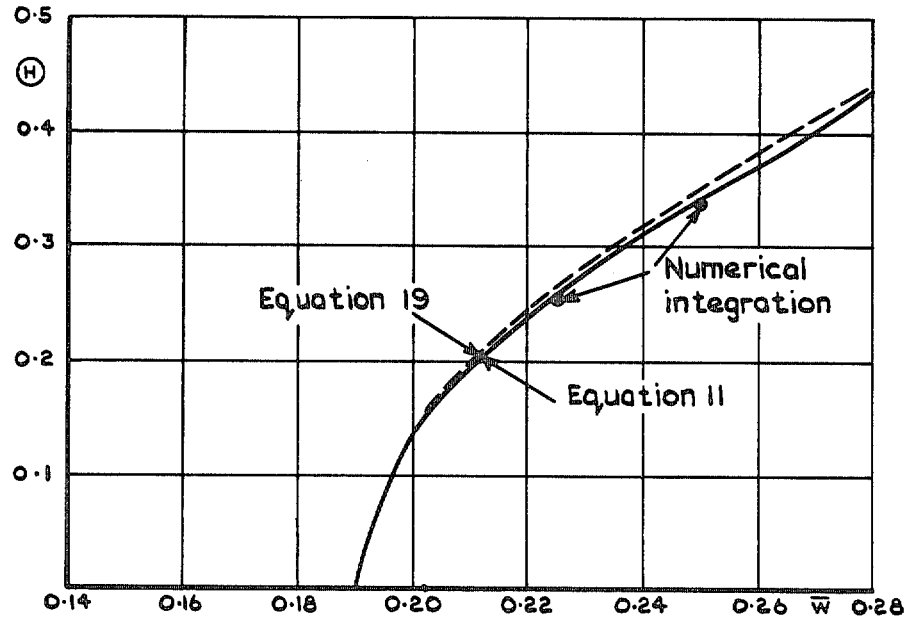

a Amplitude of steady oscillation

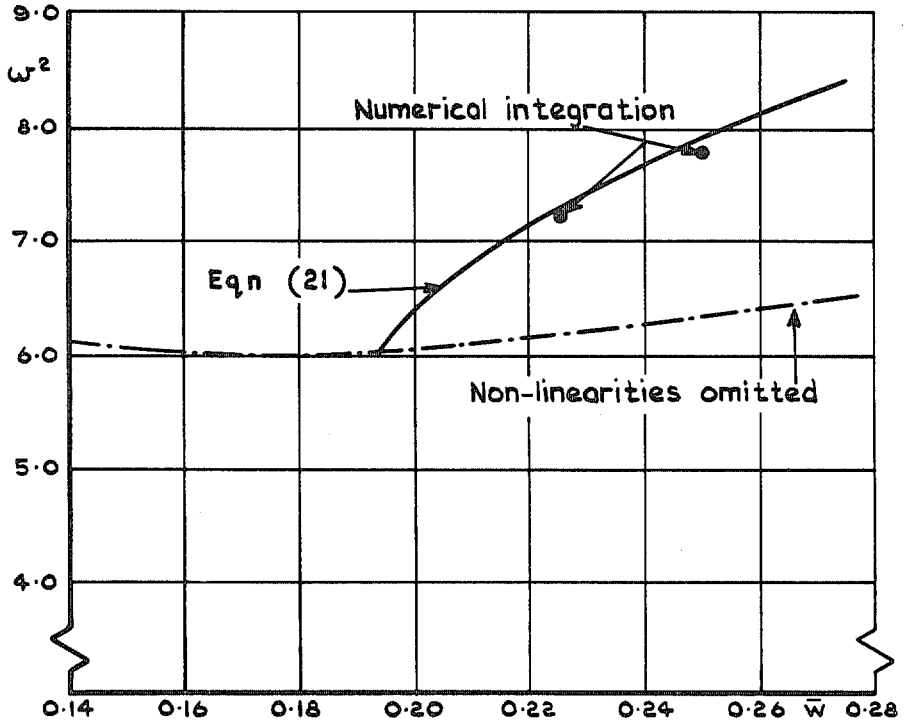

b Frequency of steady oscillation

FIG. 10a & b. Theoretical values of amplitude and frequency (HP 115 aircraft).

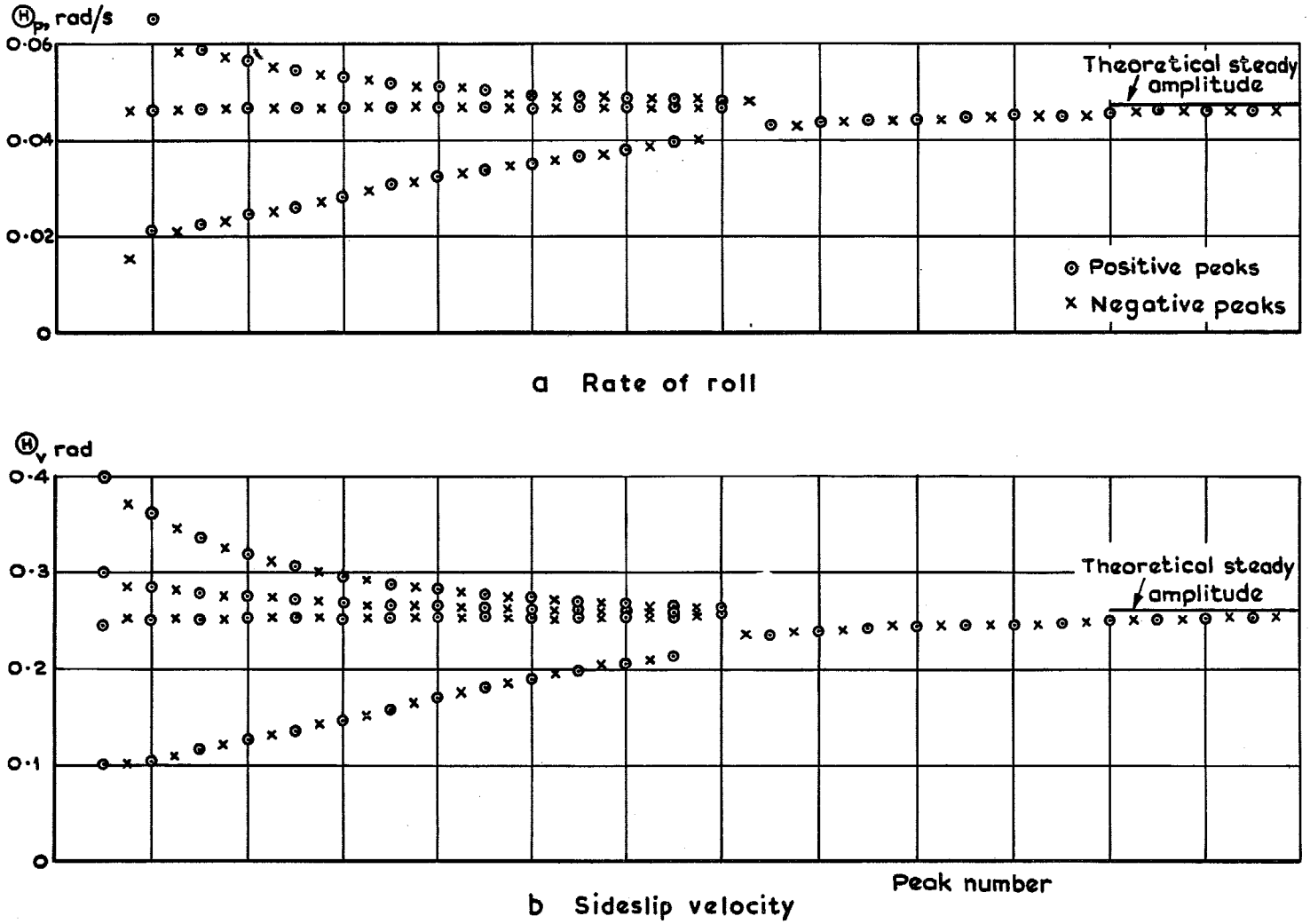

FIG. 11a & b. Computed peak values for various initial conditions, $\bar{w} = 0{\cdot}225$.

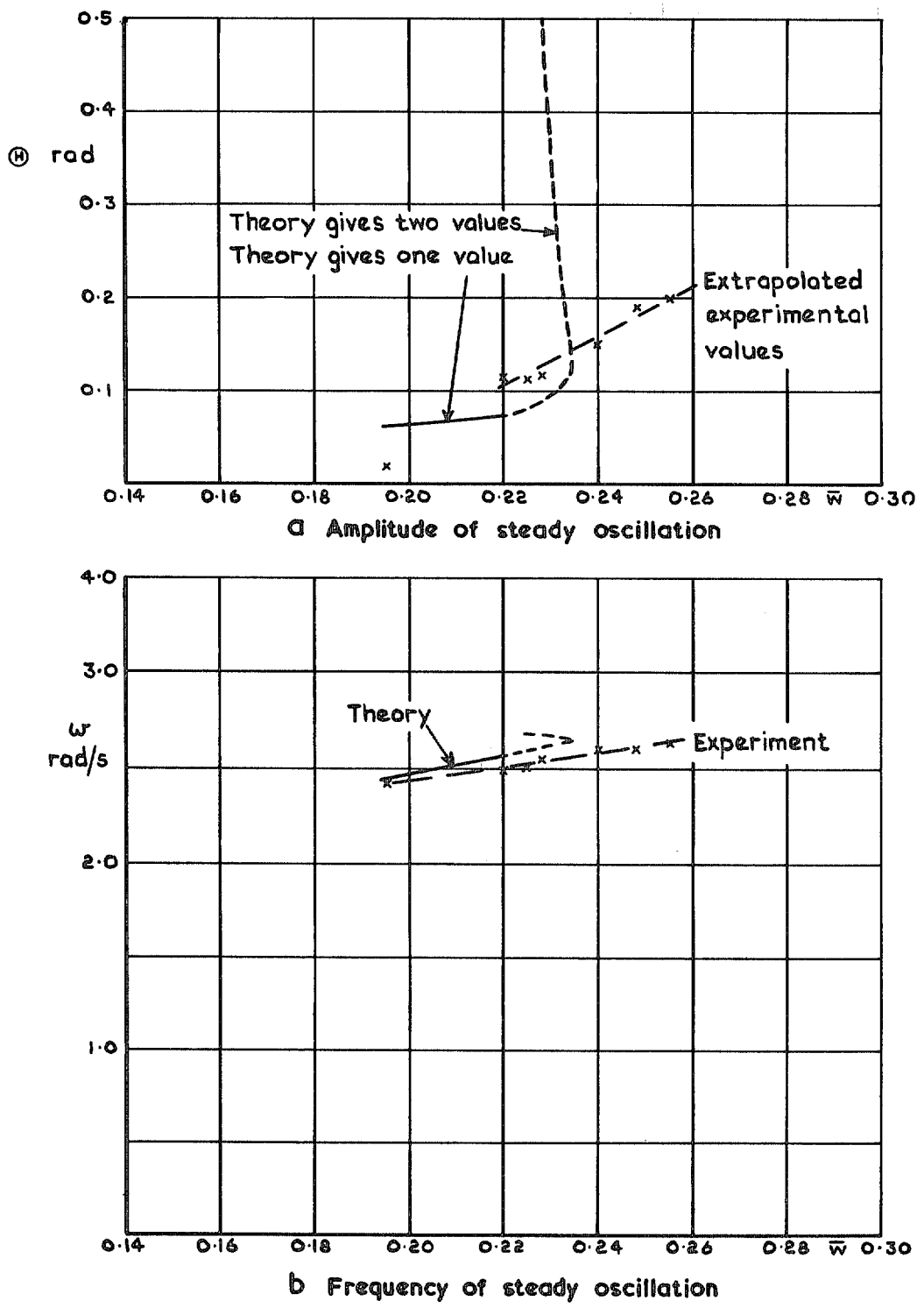

FIG. 12a & b. Comparison between experimental and theoretical values of amplitude and frequency for $C_n(\bar{v})$ represented by two straight lines.

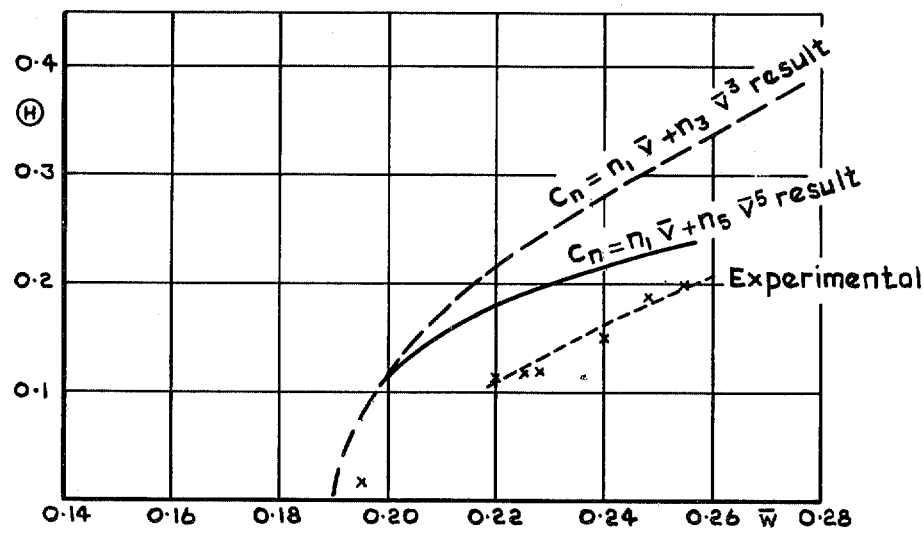

a Amplitude of steady oscillation

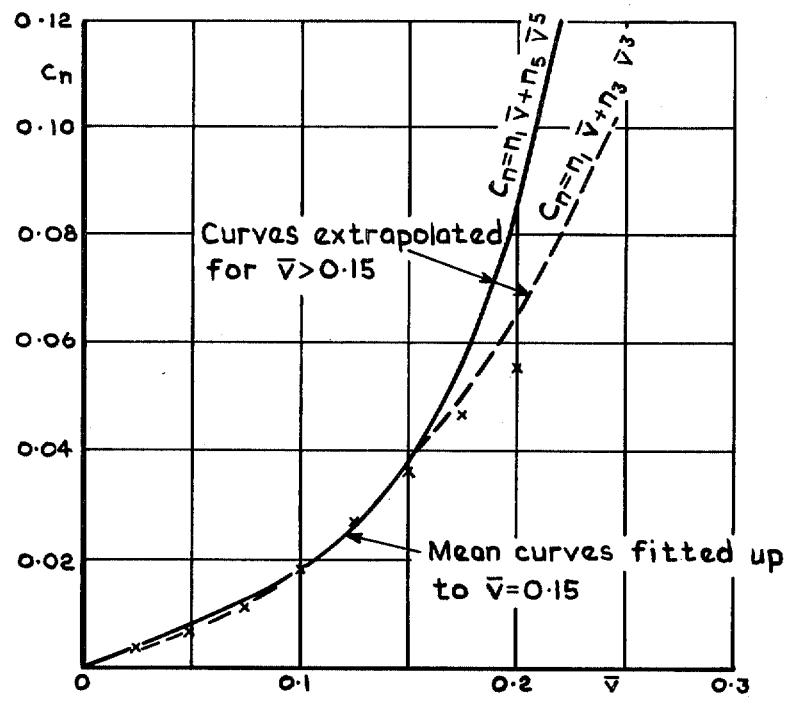

b C_n extrapolated beyond fitted values, for $\bar{w} = 0·25$

FIG. 13a & b. Comparison of polynomial representations of $C_n(\bar{v})$.

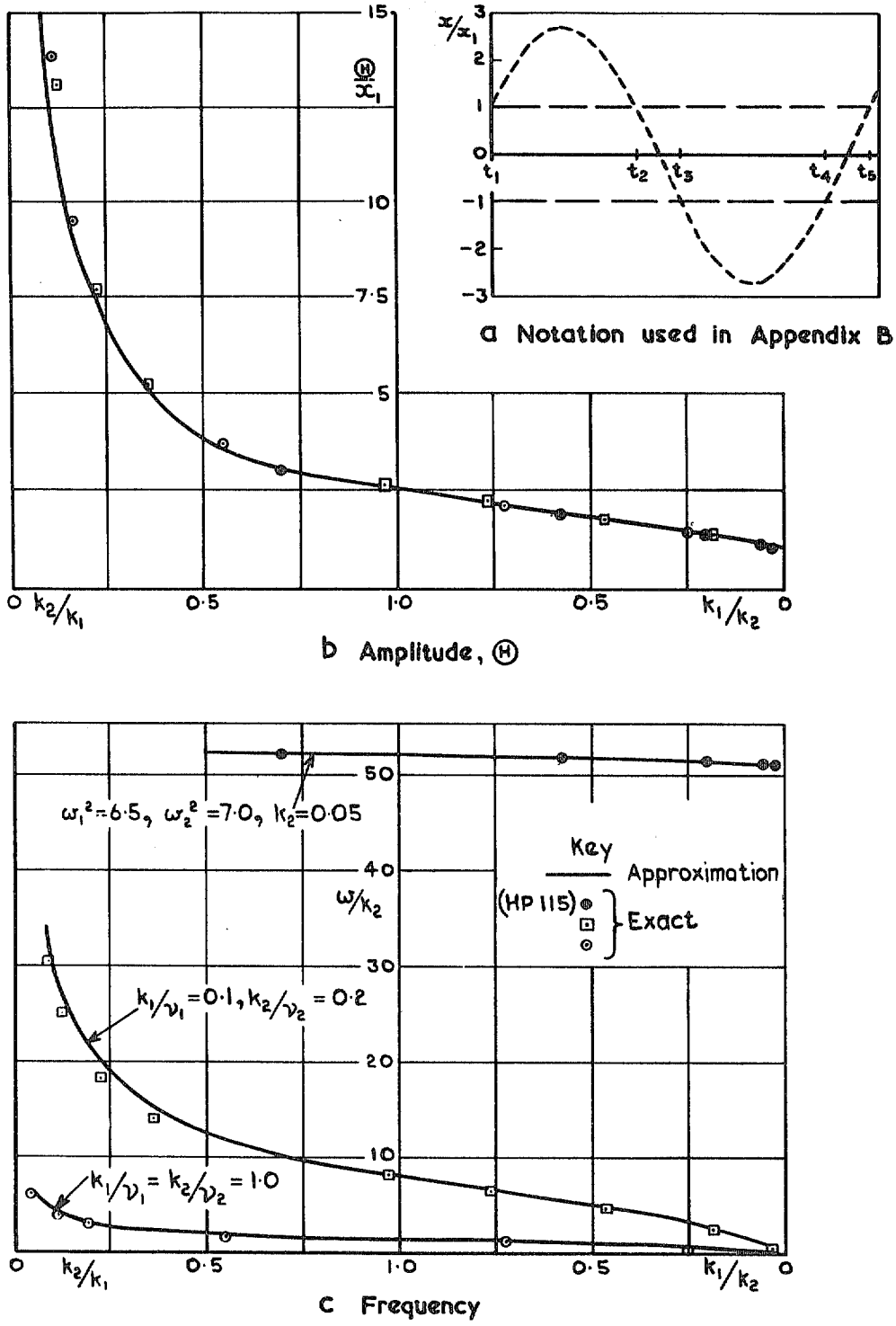

FIG. 14a–c. Comparison of exact and approximate values of amplitude and frequency of steady oscillation in second-order equation:

$$|x| < x_1,\ \ddot{x}-2k_1\dot{x}+\omega_1^2 x = 0$$
$$|x| > x_1,\ \ddot{x}+2k_2\dot{x}+\omega_2^2 x = \pm x_1(\omega_2^2-\omega_1^2).$$

Printed in Wales for Her Majesty's Stationery Office by Allens Printers (Wales) Ltd.
Dd. 502110 K.5.

Published by
HER MAJESTY'S STATIONERY OFFICE

To be purchased from
49 High Holborn, London WC1V 6HB
13a Castle Street, Edinburgh EH2 3AR
109 St Mary Street, Cardiff CF1 1JW
Brazennose Street, Manchester M60 8AS
50 Fairfax Street, Bristol BS1 3DE
258 Broad Street, Birmingham B1 2HE
80 Chichester Street, Belfast BT1 4JY
or through booksellers

R. & M. No. 3674

SBN 11 470414 7